ADAPTIVE FAULTED PHASE SELECTION FOR LINES CONNECTING CONVERTER-BASED SOURCES

Subhadeep Paladhi[1]*, Qiteng Hong[1], Campbell Booth[1]

[1]*Department of Electronic and Electrical Engineering, University of Strathclyde, Glasgow, UK*
*E-mail: subhadeep.paladhi@strath.ac.uk

Abstract

Renewable sources with numerous converter-control operations introduce dynamic fault signatures in the network. Such non-homogeneous situations result in maloperation of available phase selection methods at times, which may further lead to incorrect protection decisions and affect system resilience. In this paper, an adaptive phase selection method is proposed for lines connecting converter-based sources. Phase selection zones are formed based on the relations between faulted path sequence currents, which are unique to each fault type and remain independent of system conditions. The method uses local voltage and current data to compute an adaptive phase shift for selection zones and calculate an index based on signal availability for deriving decisions. Performance of the proposed method is evaluated on a renewable integrated 9-bus system using PSCAD/EMTDC simulation and found to be accurate and independent of converter-control operations, source types, and system conditions.

1 Introduction

Power grids are moving towards the ambitious decarbonisation target with large-scale integration of converter-interfaced renewable energy sources (CIRES) [1]. Numerous control options, embedded in the converters meeting different requirements for reliable power system operation, compel such sources to respond differently compared to conventional synchronous generators during fault [2]. The growing rate of relay maloperation following renewable integration impels to revisit every aspect associated with protection decisions [3–6]. Faulted phase selection is such a task, which is essential in deriving protection decisions like auto-reclosing, distance relaying, single-pole-tripping, etc. [7].

Relative angles between pure-fault sequence currents and voltages are generally applied in most of the available relays for phase selection [8, 9]. The principle associated with the technique is formulated considering system impedances to be homogeneous, which is not true in the presence of converter-based sources. Several training-based approaches are available in [10, 11] for fault classification. The feasibility of such schemes, requiring a large number of training data sets, is under scrutiny for application in real power systems, especially in the presence of renewable sources due to generation variability and dynamic fault pattern. A dual current controller-based phase selection technique is proposed in [12], which mimics the fault signature of a synchronous generator. Such an approach is difficult to generalize for large number of renewable sources with different converter arrangements. Correlation of transient voltage waveform can be applied for identifying faulted phases in lines connecting renewable sources [13]. Relay processors should be capable of high sampling frequency to apply such a technique. A local data-based fault classification technique is proposed in [7] for renewable connected lines considering

the grid to be strong, which may not be true always, especially following a large-scale structural or operational change in the system [14]. Remote end synchronized data may ensure correct phase selection in adverse system conditions [15]. The delay associated with data communication restricts the application of such techniques in deriving instantaneous protection decisions.

In this work, an adaptive and generalised phase selection method is proposed for lines connecting converter-interfaced renewable sources. The salient contributions of this work can be summarized as follows:

1. Phase selection zones are formed based on the relations between faulted path sequence currents (positive and negative), which are unique to each fault type and remain independent of system conditions.
2. An adaptive phase shift for selection zones is obtained using online computation of pure-fault renewable plant impedance and estimation of grid equivalent impedance during prefault to adjust with the system non-homogeneity.
3. In accordance with the signal availability at the relay point, the ratio of superimposed sequence voltages or currents (positive and negative) is applied to compute an index for deriving phase selection decisions.
4. Correct performance of the proposed method is evaluated for a renewable integrated 9-bus system using PSCAD/EMTDC simulation data. Test results with comparative assessment demonstrate the strength of the proposed method and establish it to be independent of converter-control operations, source types, and system conditions.

2 Proposed Phase Selection Method

The proposed phase selection approach is derived in this section in two stages. First, the sequence networks for different fault types are analysed to define phase selection zones. In the second stage, an index is calculated for deriving decisions.

2.1 Formulation of phase selection zones

A grid-following converter-based renewable source (RS) is generally represented with dependent current source (I_{RS}) in parallel with a variable impedance (Z_{RS}) [7], which, for each instance, can be converter to an equivalent voltage source model, as shown in Fig 1(a). This can be represented with a fixed voltage source and variable series impedance (as in Fig 1(b)), where any change in the source voltage is compensated as a voltage drop in an additional virtual impedance, included in Z_{RS}. A two bus equivalent system integrating a renewable source to grid is shown in Fig 2. A fault is created at a distance of x pu from bus M with a fault resistance R_F. The grid is represented with a voltage source (E_{Gr}) and an equivalent impedance (Z_{Gr}).
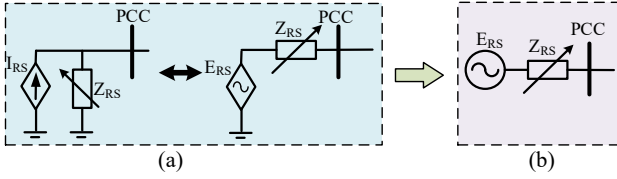

Fig. 1 Equivalent representation of converter-based sources: (a) with variable source and impedance, (b) with fixed voltage source and variable impedance.
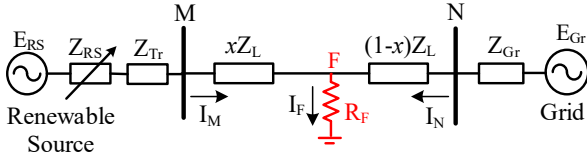

Fig. 2 Two bus equivalent system integrating a renewable source to grid.

Sequence networks for different asymmetrical fault types are provided in Fig 3. Z_S includes both Z_{RS} and Z_{Tr}. '0', '1' and '2' in subscript represent the zero, positive and negative sequence components respectively. R_{ph} is the arcing resistance between two phases. Negative sequence of a renewable plant is represented either with an open circuit or with a separate source, based on the control operation embedded in the converter. Zero sequence network is formed considering the transformer connection to be dYg. The sequence components are calculated with phase-A as reference for AG, BC and BCG faults. Phase-B is considered as reference for BG, CA and CAG faults, whereas phase-C is considered for CG, AB and ABG faults. Sequence components with different reference phases (represented with the superscripts) are related by (1), where $\alpha = e^{j\frac{2\pi}{3}}$.

$$I_{1F}^a = I_{1F}^b/\alpha^2 = I_{1F}^c/\alpha \quad and \quad I_{2F}^a = I_{2F}^b/\alpha = I_{2F}^c/\alpha^2 \quad (1)$$

Sequence networks for different fault types are analysed below to derive relations for phase selection.

2.1.1 For line-to-ground (LG) faults::
As in Fig 3(a), the positive and negative sequence currents in faulted path for LG faults are equal. Superscript 'r' represents the reference phase for sequence component calculation.
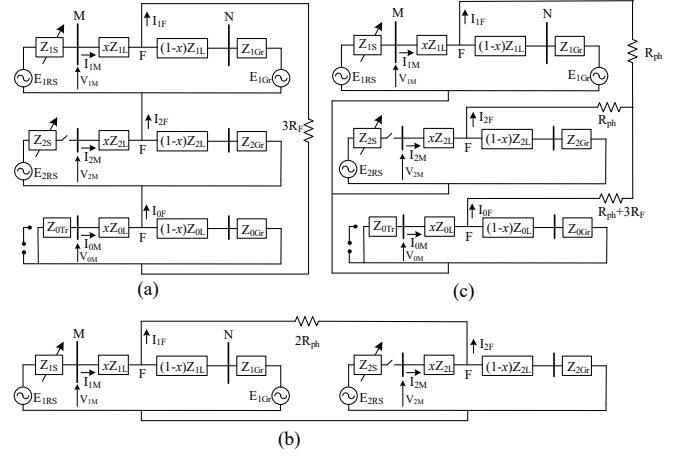
$$I_{1F}^r = I_{2F}^r \quad (2)$$

Fig. 3 Sequence network for (a) LG, (b) LL and (c) LLG faults.

Using (1), the relations between I_{1F} and I_{2F} for different LG faults are derived in (3).

$$
\begin{aligned}
For\ AG\ fault: \quad & \angle\left(I_{2F}^a/I_{1F}^a\right) = \quad 0 \\
For\ BG\ fault: \quad & \angle\left(I_{2F}^a/I_{1F}^a\right) = \quad 2\pi/3 \\
For\ CG\ fault: \quad & \angle\left(I_{2F}^a/I_{1F}^a\right) = -2\pi/3
\end{aligned}
\quad (3)
$$

2.1.2 For line-to-line (LL) faults::
I_{1F} and I_{2F} are in phase opposition for LL faults (refer Fig 3(b)).

$$I_{1F}^r = -I_{2F}^r \quad (4)$$

Using (1), the relations between I_{1F} and I_{2F} for different LL faults are derived in (5).

$$
\begin{aligned}
For\ BC\ fault: \quad & \angle\left(I_{2F}^a/I_{1F}^a\right) = \quad \pi \\
For\ CA\ fault: \quad & \angle\left(I_{2F}^a/I_{1F}^a\right) = -\pi/3 \\
For\ AB\ fault: \quad & \angle\left(I_{2F}^a/I_{1F}^a\right) = \quad \pi/3
\end{aligned}
\quad (5)
$$

2.1.3 For line-to-line-to-ground (LLG) faults::
As in Fig 3(c), the sequence currents in the faulted path for LLG faults are related by (6).

$$I_{1F}^r = -\left(I_{2F}^r + I_{0F}^r\right) \quad (6)$$

Negative and zero sequence impedance angles are almost equal in a transmission network, which results in I_{2F}^r and I_{0F}^r to be in same phase. Thus, I_{1F}^r and I_{2F}^r are considered almost in phase opposition, similar to LL faults and the relations derived in (5) remain valid even with ground involvement. Relations obtained in (3) and (5) are consistent for any system conditions and form the phase selection zones, as shown in Fig 4. Considering measurement inaccuracy in real power systems, a margin of $\pm 15°$ is provided for each zone.
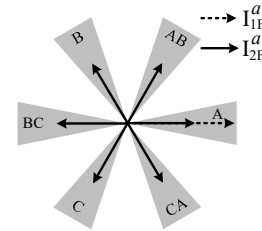

Fig. 4. System independent phase selection zones

2.2 Formulation of the phase selection technique

A pure-fault positive sequence network is introduced in Fig 5 [3]. Pure-fault components (ΔV_{1M} and ΔI_{1M}) are obtained in (3). 'f' and 'pre' in superscript represent measurements during fault and prefault respectively.

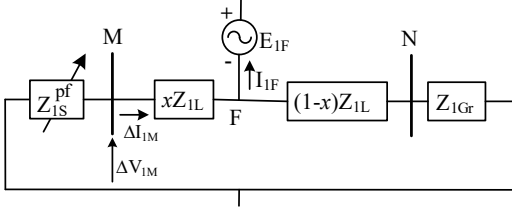$$\Delta V_{1M} = V_{1M}^f - V_{1M}^{pre} \text{ and } \Delta I_{1M} = I_{1M}^f - I_{1M}^{pre} \quad (7)$$

Fig. 5. Pure-fault positive sequence network.

Applying current distribution principle in Fig 5, ΔI_{1M} is expressed in terms of I_{1F} in (8).

$$\Delta I_{1M} = \frac{(1-x)Z_{1L} + Z_{1Gr}}{Z_{1S}^{pf} + Z_{1L} + Z_{1Gr}} I_{1F} \quad (8)$$

Z_{1S}^{pf} represents the pure-fault impedance of the renewable plant (including transformer) and can be obtained by,

$$Z_{1S}^{pf} = -\frac{\Delta V_{1M}}{\Delta I_{1M}}. \quad (9)$$

Using (9), the relation in (8) can be rewritten as in (10).

$$\Delta V_{1M} = -\frac{Z_{1S}^{pf}((1-x)Z_{1L} + Z_{1Gr})}{Z_{1S}^{pf} + Z_{1L} + Z_{1Gr}} I_{1F} \quad (10)$$

For renewable plants with balanced current controlled converter, negative sequence equivalent is represented with an open circuit. Thus, local negative sequence voltage is same as the fault point voltage and expressed as in (11).

$$\Delta V_{2M} = -I_{2F}((1-x)Z_{1L} + Z_{1Gr}) \quad (11)$$

For renewable interfacing converters with dual current controller, ΔI_{2M} can be expressed in terms of I_{2F}, as in (12). Negative sequence impedance is considered to be same as the positive sequence impedances for both line and grid.

$$\Delta I_{2M} = \frac{(1-x)Z_{2L} + Z_{2Gr}}{Z_{2S}^{pf} + Z_{2L} + Z_{2Gr}} I_{2F} = \frac{(1-x)Z_{1L} + Z_{1Gr}}{Z_{2S}^{pf} + Z_{1L} + Z_{1Gr}} I_{2F} \quad (12)$$

Using (10) and (11), the ratio of pure-fault sequence voltages is obtained in (13), which indicates the faulted path sequence current ratio (as derived in Section 2.1), shifted by an angle θ_1^{sh}.

$$\frac{\Delta V_{2M}}{\Delta V_{1M}} = \left(\frac{Z_{1S}^{pf} + Z_{1L} + Z_{1Gr}}{Z_{1S}^{pf}}\right)\left(\frac{I_{2F}}{I_{1F}}\right) = \left(\frac{I_{2F}}{I_{1F}}\right)e^{j\theta_1^{sh}} \quad (13)$$

where $\theta_1^{sh} = arg\left(\frac{Z_{1S}^{pf} + Z_{1L} + Z_{1Gr}}{Z_{1S}^{pf}}\right)$.

Using (8) and (12), the ratio of pure-fault sequence currents is obtained in (14), which indicates the faulted path sequence current ratio (as derived in Section 2.1), shifted by an angle θ_2^{sh}.

$$\frac{\Delta I_{2M}}{\Delta I_{1M}}\left(\frac{Z_{1S}^{pf} + Z_{1L} + Z_{1Gr}}{Z_{2S}^{pf} + Z_{1L} + Z_{1Gr}}\right)\left(\frac{I_{2F}}{I_{1F}}\right) = \left(\frac{I_{2F}}{I_{1F}}\right)e^{j\theta_2^{sh}} \quad (14)$$

where $\theta_2^{sh} = arg\left(\frac{Z_{1S}^{pf} + Z_{1L} + Z_{1Gr}}{Z_{2S}^{pf} + Z_{1L} + Z_{1Gr}}\right)$.

Computation of θ_1^{sh} and θ_2^{sh} requires Z_{1S}^{pf}, Z_{2S}^{pf} Z_{1L} and Z_{1Gr}. Z_{1L} is available using system data. Z_{1S}^{pf} is calculated using (9). Z_{2S}^{pf} can be calculated similar to (9), using negative sequence measurements. Applying the Thevenin equivalent estimation approach available in [16], Z_{1Gr} can be determined using three consecutive voltage and current measurement sets at bus M, obtained at different instances during prefault. Considering the grid to be dominated by synchronous generators, Z_{1Gr} estimated during prefault remains unchanged during fault.

2.3 Implementation of the proposed approach

Steps associated with the implementation of the proposed phase selection approach are provided in Fig 6. Z_{1Gr} is estimated using local voltage and current data during prefault, and updated continuously until fault detection. Following fault detection, negative sequence current and voltage are checked. With both having negligible values, relay detects all the three phases to be faulted. In the presence of V_{2M} with negligible I_{2M}, relay first calculates θ_1^{sh} and applies to rotate the phase selection zones accordingly. Then, the relay computes $\angle\left(\frac{\Delta V_{2M}}{\Delta V_{1M}}\right)$ and compares with the shifted zones to identify faulted phases. For converters having dual sequence current controller i.e. in the presence of I_{2M}, relay calculates θ_2^{sh} and rotates the phase selection zones accordingly. Then, the relay computes $\angle\left(\frac{\Delta I_{2M}}{\Delta I_{1M}}\right)$ and compares it with the newly shifted zones to derive proper phase selection decision.
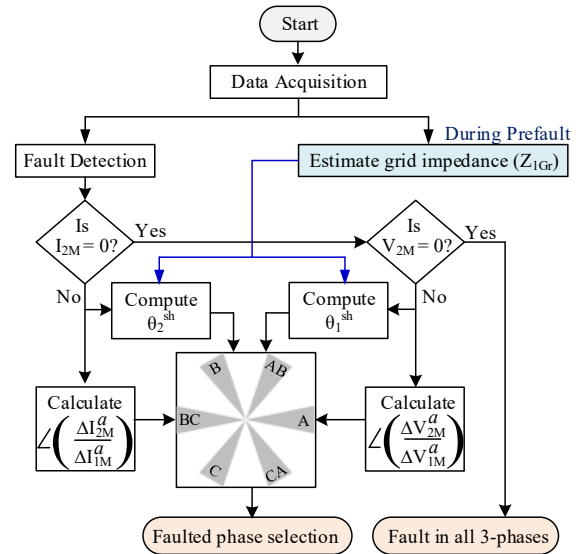

Fig. 6. Flow chart of the proposed phase selection approach.

3 Results

Performance of the proposed phase selection method is evaluated on a 230 kV, 60 Hz, renewable integrated 9-bus system, as shown in Fig 7. Simulations are carried out using PSCAD/EMTDC platform. Voltage and current phasors are estimated using 1-cycle discrete Fourier transform (DFT) with a sampling frequency of 3.84 kHz. A 200 MVA solar PV source is connected at bus 3 through dYg transformer. The solar plant inverter is controlled in synchronous reference frame with feedforward control and operates close to unity power

Table 1 Performance evaluation for different test conditions

Fault Specification	Case Overview		Phase Selection Zone (Actual)			Shifted Zone (Proposed)			δ
AG ($R_F = 5\Omega$)	Change in converter control	Balanced current control	$-15°$	to	$-15°$	$-32.7°$	to	$-2.7°$	$-17.5°$
		Dual current control	$-15°$	to	$15°$	$37.8°$	to	$67.8°$	$53.1°$
AB ($R_{ph} = 1\Omega$)	Change in grid codes	Unity power factor	$45°$	to	$75°$	$52.7°$	to	$82.7°$	$67.4°$
		Reactive current priority	$45°$	to	$75°$	$-148.4°$	to	$-118.4°$	$-133.2°$
CG ($R_F = 50\Omega$)	Grid strength variation	Strong grid	$-135°$	to	$-105°$	$-152.2°$	to	$-122.2°$	$-137.4°$
		Weak grid	$-135°$	to	$-105°$	$142.5°$	to	$172.5°$	$157.2°$
BCG ($R_F = 10\Omega$)	Different fault distance from bus 3	$0.1\ pu$	$165°$	to	$-165°$	$124.4°$	to	$154.4°$	$139.7°$
		$0.5\ pu$	$165°$	to	$-165°$	$98.1°$	to	$128.1°$	$112.9°$
		$0.9\ pu$	$165°$	to	$-165°$	$158.9°$	to	$-171.1°$	$174.1°$
CAG ($R_F = 10\Omega$)	Different renewable sources	Solar PV	$-75°$	to	$-45°$	$102.3°$	to	$132.3°$	$117.4°$
		Type-III wind	$-75°$	to	$-45°$	$-21.2°$	to	$8.8°$	$-5.5°$
		Type-IV wind	$-75°$	to	$-45°$	$37.3°$	to	$67.3°$	$52.7°$

factor. However, the proposed method is tested for different converter controls, grid code requirements, grid strength, and source types.
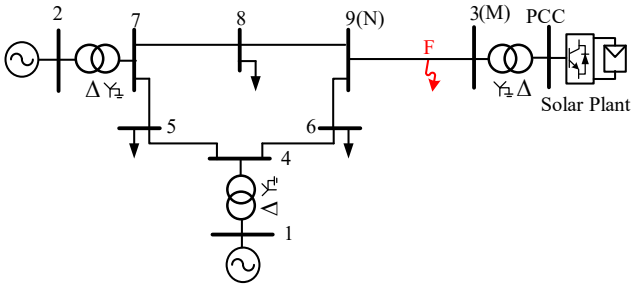

Fig. 7. Renewable integrated 9-bus test system.

Fig. 8 Superimposed sequence voltage ratio angle with phase selection zones.

An AG fault is created in the line 3-8 of the system in Fig 7 at a distance of $0.4\ pu$ from bus 3 with a fault resistance of $15\ \Omega$. Phase selection methods are tested for the relay at bus 3. The solar plant, being controlled with a balanced current controller, does not generate negative sequence current, even for such an asymmetrical fault situation. The proposed method computes the angle θ_1^{sh} and rotates the phase selection zones accordingly. Following the zone shift, the relay calculates the superimposed sequence voltage ratio angle (δ) to identify the faulted phase. The result is provided in Fig 8, which shows that the relay fails to identify the faulted phase correctly with the conventional fixed phase selection zone. This indicates a clear maloperation of the method in [8]. It can be observed that δ obtains a value within the shifted zone, as proposed in this work and identifies the faulted phase correctly for the situation, even during the transient period within one cycle. This demonstrates the superiority of the proposed method, compared to the conventional approach.

Performance of the proposed method is also evaluated for different test conditions. The observations are provided in Table 1 and summarised below.
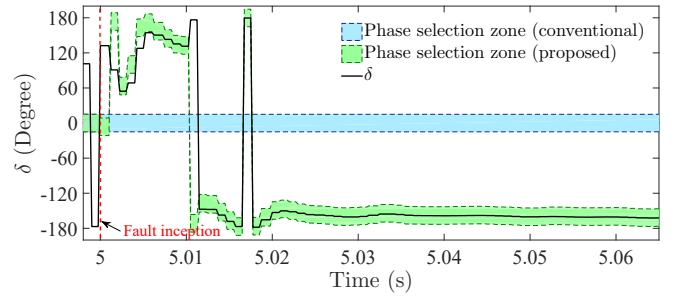
1. In case-1, the solar plant inverter is controlled with a balanced and a dual current controller, one at a time. The balanced controller generates only positive sequence current, even during unbalanced faults, whereas the inverter with a dual current controller generates both positive and negative sequence currents.

2. Grid code requirements influence the fault characteristics significantly. In case-2, two grid codes are complied with the inverter control, one at a time. With the first one, the solar plant operates close to unity power factor, even during fault. The second grid code prioritizes reactive current generation from the inverter during fault.

3. Available phase selection methods are influenced by grid strength [7, 8]. Therefore, the performance of the proposed method is evaluated for two different grid strengths. First, the method is tested for 9-bus system with its full strength. Later, the generator at bus 2 is disconnected to make the grid weak (loads are adjusted to maintain stability during non-fault situations).

4. Fault severity varies with its location and influences the control operation of converter-based sources accordingly. In case-4, the method is tested for faults created at different locations in line 3-9.

5. In order to verify the source independence of the proposed method, the solar plant connected at bus 3 is replaced with a Type-III and Type-IV wind farm of the same capacity, one at a time.

Results provided in Table 1 show that δ obtains a value outside the conventional phase selection zones, for most of the cases. This indicates clear maloperations of the conventional phase selection approach [8] for lines connecting converter-based sources. As in Column-IV of Table 1, the shifted zones, obtained through the proposed approach, cover δ in all cases and identify the faulted phases correctly.

4   Conclusion

Converter-based sources with different control options result in non-homogeneous fault characteristics in renewable integrated power networks. Such situations lead to incorrect performance of available phase selection techniques. An adaptive faulted phase selection method is proposed for such non-homogeneous power networks integrating renewable sources. Using the relation between faulted path sequence current angles, the proposed method obtains system-independent phase selection zones. Based on signal availability at the relay point, superimposed voltage or current ratio is computed to trace the phase selection zones, which are adjusted with the system non-homogeneity, by applying a shift angle computed using local data. Results are provided for variations in fault types, fault resistance, fault location, converter control operation, grid code compliance, grid strength, and renewable type. This demonstrates the adaptivity of the proposed method with the change in fault signature in the network. Comparative assessment with the conventional technique reveals the strength of the proposed method.

5   Acknowledgements

6   References

[1] 'Renewables Integration in India' (NITI Ayog, International Energy Agency, 2021).

[2] Du, W., et al.: 'Modeling of Grid-Forming and Grid-Following Inverters for Dynamic Simulation of Large-Scale Distribution Systems', IEEE Trans. Power Del., 2021, 36, (4), pp 2035-2045.

[3] Paladhi, S., Pradhan, A. K.: 'Adaptive distance protection for lines connecting converter-interfaced renewable plants', IEEE J. Emerg. Sel. Topics Power Electr., 2021, 9, (6), pp. 7088–7098.

[4] Jia, K., Yang, Z., Fang, Y., Bi, T., Sumner, M.: 'Influence of inverter-interfaced renewable energy generators on directional relay and an improved scheme', IEEE Trans. Power Electr., 2019, 34, (12), pp. 11843–11855.

[5] Chowdhury, A., Paladhi, S., Pradhan, A. K.: 'Adaptive unit protection for lines connecting large solar plants using incremental current ratio', IEEE Syst. J., 2022, 16, (2), pp. 3272–3283.

[6] Paladhi, S.; Hong, Q.; Booth, C. D.: 'Adaptive distance protection for multi-terminal lines connecting converter-interfaced renewable energy sources', IET Conference Proceedings, 2022, p. 31-35.

[7] Paladhi, S., Pradhan, A. K.: 'Adaptive fault type classification for transmission network connecting converter-interfaced renewable plants', IEEE Syst. J., 2021, 15, (3), pp. 4025–4036.

[8] Kasztenny, B., Campbell, B., Mazereeuw, J., 'Phase selection for single-pole tripping - weak infeed conditions and cross country faults' (GE Power Management, 2000), pp. 1–19.

[9] Roberts, J. B., Schweitzer III, E. O.: 'Fault identification system for use in protective relays for power transmission lines'. US Patent 5,515,227, May 1996.

[10] Reddy, M. J., Mohanta, D. K.: 'Adaptive-neuro-fuzzy inference system approach for transmission line fault classification and location incorporating effects of power swings', IET Gen., Trans., Dist., 2008, 2, (2), pp. 235–244.

[11] Jena, M. K., Samantaray, S. R.: 'Data-mining-Bbased intelligent differential relaying for transmission lines including UPFC and wind farms', IEEE Trans. Neural Net. Learn. Syst., 2016, 27, (1), pp. 8–17.

[12] Azzouz, M. A., Hooshyar, A.: 'Dual current control of inverter-interfaced renewable energy sources for precise phase selection', IEEE Trans. Smart Grid, 2019, 10, (5), pp. 5092–5102.

[13] Song, G., Wang, C., Wang, T., Kheshti, M., Kang. X.: 'A phase selection method for wind power integration system using phase voltage waveform correlation', IEEE Trans. Power Del., 2017, 32, (2), pp. 740–748.

[14] Paladhi, S., Pradhan, A. K.: 'Adaptive zone-1 setting following structural and operational changes in power system', IEEE Trans. Power Del., 2018, 33, (2), pp. 560–569.

[15] Swain, K. B., Mahato, S. S., Cherukuri, M.: 'Expeditious situational awareness-based transmission line fault classification and prediction using synchronized phasor measurements', IEEE Access, 2019, 7, pp. 168187–168200.

[16] Paladhi, S., Pradhan, A. K.: 'Resilient protection scheme preserving system integrity during stressed condition', IET Gen., Trans., Dist., 2019, 13, (14), pp. 3188–3194.